Determination of the Aerodynamic Characteristics of the Mission Adaptive Wing

Stephen B. Smith*
Air Force Flight Test Center, Edwards Air Force Base, California
and
David W. Nelson†
Boeing Advanced Systems, Seattle, Washington

The Advanced Fighter Technology Integration F-111 flight research program was conducted to develop and demonstrate the potential technology enhancements of the mission adaptive wing. This wing incorporated smooth contour, variable-camber leading- and trailing-edge surfaces that could modify wing contour in flight by means of an internal linkage system and flexible skins. Extensive wind-tunnel and flight test data were gathered during the course of the program to define the aerodynamic performance benefits attributed to the mission adaptive wing. Full-scale aerodynamic characteristics and predicted performance were initially based on a wind-tunnel data base. Flight testing was conducted to determine lift, drag, buffet, and wing upper and lower surface pressures. The flight test data served to verify the wind-tunnel predictions and to provide a data base for follow-on analyses.

Nomenclature

BL	= buttock line
C_D	= coefficient of drag
C_L	= coefficient of lift
$C_{L_{\delta f}}$	= flap effectiveness (lift)
C_M	= coefficient of pitching moment
C_N	= normal force coefficient
$dC_M/d\delta h$	= horizontal tail effectiveness
$EC_{L_{\delta f}}$	= elastic-to-rigid flap effectiveness ratio
F_e	= engine ram drag
F_g	= engine gross thrust
i_t	= incidence angle of the engine relative to the fuselage
i_{wb}	= incidence angle of the wing box relative to the fuselage
MAC	= wing mean aerodynamic chord (10.5 ft)
n_x, n_z	= aircraft acceleration; along flightpath, normal to flightpath
q	= dynamic pressure
S	= reference wing area
$TEFS$	= trailing-edge flap position
α, α_w	= angle of attack; relative to fuselage, relative to wing chord
δh	= horizontal tail position
Λ	= wing sweep position

Subscript

δf	= flap position

Superscripts

E	= elastic
R	= rigid

Presented as Paper 88-2556 at the AIAA 6th Applied Aerodynamics Conference, Williamsburg, VA, June 6–8, 1988; received April 29, 1989; revision received Dec. 6, 1989.

*Project Manager, Research Projects Division.
†Senior Specialist Engineer. Member AIAA.

Introduction

THE Advanced Fighter Technology Integration (AFTI) F-111 was a joint Air Force/NASA/Boeing venture to develop smooth, variable-camber wing technology. Under the direction of the Air Force Wright Research and Development Center, Boeing Advanced Systems designed and fabricated the mission adaptive wing (MAW). This experimental wing was a unique design alternative to conventional, hinged flaps. By combining variable camber with variable sweep and an automatic flight control system, the MAW was designed to be capable of near-optimum wing performance throughout the flight envelope. The MAW was the successor to the Transonic Aircraft Technology (TACT) program, which explored the benefits of a supercritical wing design in a flight research program conducted between 1972 and 1976.

The testbed aircraft, which was modified by addition of the MAW, was a preproduction F-111A with a variable wing sweep range of 16–58 deg. The aircraft was highly instrumented to provide precise measurements for a number of aerodynamic and flight control research applications. The flight test portion of the research program was conducted between 1985 and 1988.

The MAW system consisted of variable-camber leading- and trailing-edge flaps, flap actuation linkages, hydraulic motors and mechanical actuators, and duel redundant computers to control flap position. Six independent trailing-edge (TE) flap segments (three per wing) and two leading-edge (LE) flap segments provided smooth, continuously variable wing camber using flexible fiberglass skins on the upper surface and sliding panels on the lower surface. The upper surfaces were smooth and continuous, and no gap or discontinuities were created when the leading and trailing edges were deflected. The flaps had a range of travel of about 1 deg up to about 20 deg down. All six trailing-edge flap segments were deflected in unison. The mid and outboard trailing-edge segments, however, could also be deflected independently to supplement the roll control provided by differential movement of the F-111 horizontal stabilizer. With the flaps positioned at 0-deg leading edge and 2-deg trailing edge (a camber of 0/2), the wing camber was very similar to the TACT wing. The wing airfoil shape, however, was a refined version of the TACT supercritical airfoil.

The MAW control system had two basic operating modes: manual and automatic. In the manual mode, the pilot could position the LE and TE flaps anywhere within their range of

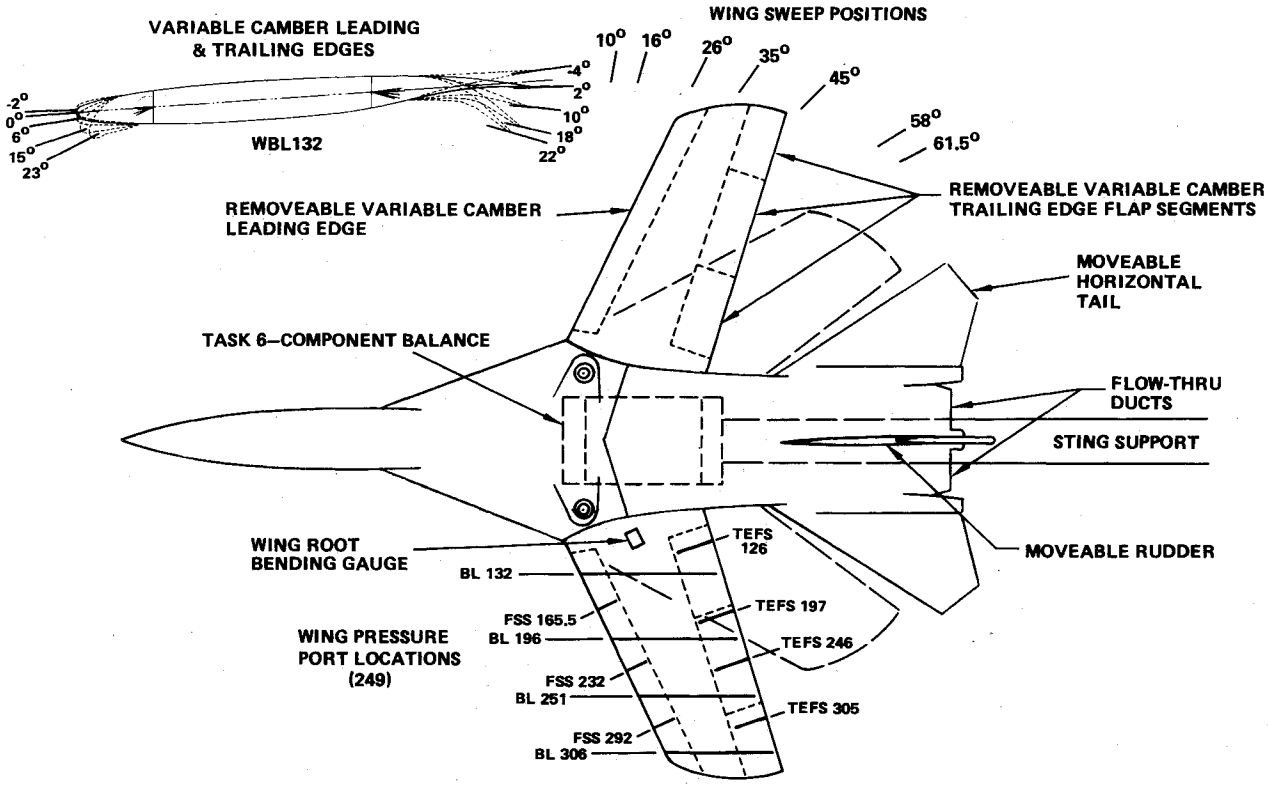

Fig. 1 AFTI/F-111 1/12-scale wind-tunnel model.

travel by use of a cockpit control panel. The majority of the flight test performance data were gathered at these manually selected camber positions. In the automatic operating mode, the pilot could select from four control modes that continuously repositioned the flaps in response to desired control functions. One of the modes, maneuver camber control (MCC), was of interest for this study because it directly affected aircraft performance. The MCC automatic mode was designed to provide a practical means of setting the optimum camber to maximize performance during maneuvering flight. It positioned the LE and TE flaps to provide the optimum camber for minimum drag as a function of lift coefficient and Mach number. The algorithm used stored table data of wind-tunnel predicted values of camber.[1]

During the design phase, wind-tunnel data were used to predict the aerodynamic characteristics of the AFTI/F-111 with the MAW. Flight test data were obtained to validate the wind-tunnel estimates and to demonstrate that the predicted benefits of the MAW were achievable through means of an automatic control system. The wind-tunnel and flight test analyses that led to a definition of the lift and drag characteristics of the aircraft are described in this paper.

Wind-Tunnel Investigations

An extensive wind-tunnel test program was conducted to 1) verify predicted aerodynamic performance benefits of the smooth skin variable-camber wing; 2) establish an aerodynamic data base for flight control, structural, and mechanical design; and 3) satisfy safety of flight requirements for the flight test program. Because of the large number of configuration variables required to adequately model a variable-camber, variable-sweep wing system it was necessary to devise techniques to ensure efficient use of wind-tunnel test time. These techniques included supplementing the wind-tunnel data with theoretical analysis, especially with regard to predicting flexibility effects, and utilizing a simple trim routine (based on extracted tail polars) to reduce the amount of tail deflection test data required.

Wind-Tunnel Aerodynamic Data Base

The AFTI/F-111 wind-tunnel test program encompassed a total of 1484 occupancy hours in both NASA and Air Force tunnels. Test conditions covered a Mach number range from 0.25 to 2.50 and Reynolds numbers from 1.8 to 7.8×10^6/ft (based on MAC). The test article (Fig. 1) was a 1/12 scale model of rigid steel construction that allowed testing at high Reynolds number/high Mach number conditions. A sting mounting system was employed, and aerodynamic forces and moments were measured by means of an internal, six component, strain gauge balance. The model was also instrumented with static pressure orifices located on the wing upper and lower surfaces, as shown in Fig. 1, and a wing root bending moment gauge. Configuration variables included variable wing sweep and discrete variable-camber flap deflections simulated by removable wing leading- and trailing-edge segments.

A number of adjustments were made to correct the wind-tunnel data to full-scale conditions. This paper specifically addresses those adjustments made to account for the distinct flexibility characteristics of the full-scale AFTI variable-camber wing. The thrust/drag force accounting system used to predict full-scale, variable-camber envelope drag polars is also described.

Flexibility Corrections

The unique AFTI/F-111 aeroelastic properties were derived from the fact that the variable-camber wing was built around the same wing box and pivot structures as the original TACT wing. When the variable-camber leading and trailing edges were undeflected, AFTI and TACT had similar planforms and airfoil shapes and, therefore, similar span and chordwise load distributions. Deflection of the variable-camber flaps, however, could cause loadings that were different from those for which the wing box was designed. The result was that very large wing box deflections could occur, especially in torsion. As an example, Fig. 2 shows the predicted wing box elastic twist increment for several combinations of leading- and trailing-edge deflections. Trailing-edge deflection is seen to be the

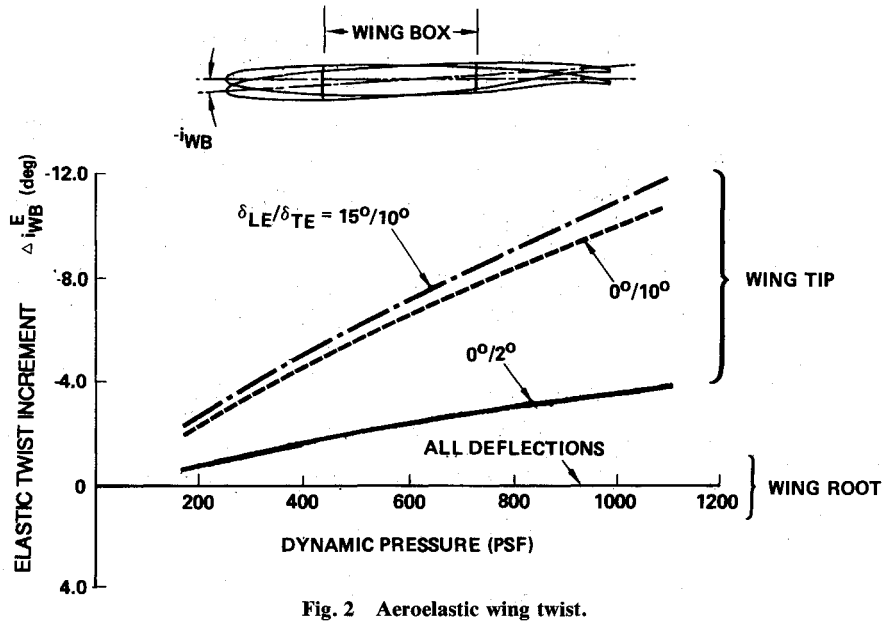

Fig. 2 Aeroelastic wing twist.

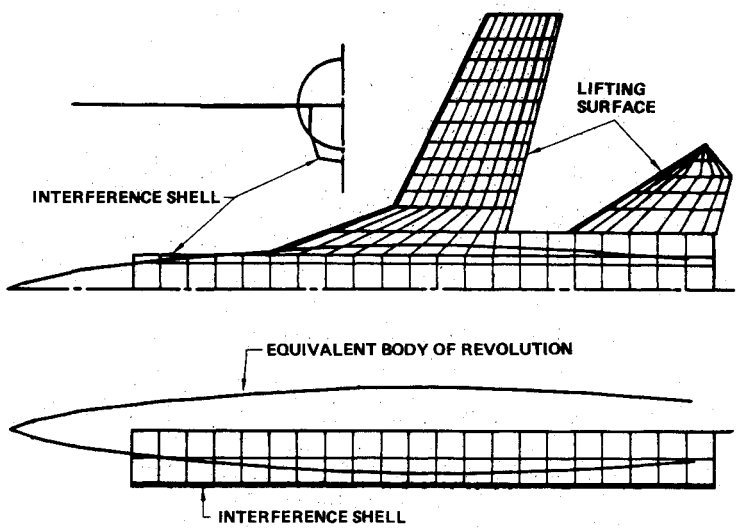

Fig. 3 FLEXSTAB aerodynamic model, sweep = 26 deg.

primary driver and tends to wash out the wing tips as dynamic pressure is increased. In the example shown, at dynamic pressures corresponding to high speed, low-level flight, the elastic twist increment at the wing tip is on the same order of magnitude as the trailing-edge flap deflection.

A theoretical FLEXSTAB[2] model was developed to simulate the aeroelastic properties of the full-scale AFTI/F-111 aircraft and to derive a set of flexibility corrections to apply to the rigid wind-tunnel model data base. FLEXSTAB is a system of computer codes that use linear theories to solve for aerodynamic forces and moments, inertial loads, and structural deflections simultaneously. The aerodynamic and structural formulation in FLEXSTAB is based on finite element models and influence coefficient matrices. Elements of the three-dimensional, aerodynamic influence coefficient matrix are derived using the constant pressure panel method developed by Woodward.[3] Aerodynamic loads are obtained by integrating pressures over the panel areas, assuming each discrete load acts normal to the surface at the panel centroid. The distribution of panels employed in the AFTI FLEXSTAB model is shown in Fig. 3.

FLEXSTAB is a simple, fast, and efficient analytical tool; however, the limitations imposed by linear theory are severe. Panel incidence angles must be kept small, thereby limiting both angle of attack and large leading- and trailing-edge flap deflection angles. Furthermore, linear theory cannot model viscous effects and discontinuities in the transonic flowfield such as local shock wave interactions. These limitations were minimized, in part, by deriving aeroelastic corrections to the rigid model wind-tunnel data rather than trying to determine absolute values of the elastic aerodynamic coefficients and by adjusting the aeroelastic corrections with wind-tunnel derived factors.

Both a rigid model, representing the wind-tunnel wing twist and camber, and an elastic model with a full-scale structural representation were analyzed by FLEXSTAB. Elastic corrections were obtained by incrementing or "ratioing" the predicted aerodynamic coefficients for both models. Since the AFTI cruise (0/2 camber) wing and TACT wing had similar planforms and airfoil shapes, as well as sharing the same wind box and pivot structures, it was possible to validate this approach by comparing FLEXSTAB results with TACT flight test data. Figure 4 is an example showing the good correlation obtained for the normal force elastic-to-rigid ratio at a transonic flight condition.

An example of the linear theory limitations for large flap deflections is given in Fig. 5 where predicted and wind-tunnel

measured trailing-edge flap effectiveness are compared. Linear theory did not predict the loss in trailing-edge effectiveness, due to viscous related effects, seen in the wind-tunnel data as the trailing edge was deflected. To account for this deficiency, the FLEXSTAB-derived elastic-to-rigid ratio for flap effectiveness was adjusted by wind-tunnel measured flap effectiveness as shown by Eqs. (1) and (2).

$$C_{L_{\delta f}} = EC_{L_{\delta f}} \times (C_{L_{\delta f}})_{wt} \tag{1}$$

where

Theoretical:

$$EC_{L_{\delta f}} = (C_{L_{\delta f}})^E/(C_{L_{\delta f}})^R \tag{2}$$

Similar wind-tunnel derived adjustments were made to the theoretical elastic-to-rigid ratios for other flap deflection or wing twist dependent aerodynamic coefficients.

Thrust/Drag Force Accounting System

The force accounting system, diagramed in Fig. 6, was used to identify all thrust, drag, and interacting forces and to account for these forces when adjusting the wind-tunnel data to full-scale levels. This system was originally developed for the TACT supercritical wing program and then refined to account for the uniqueness of the AFTI/F-111 smooth, variable-camber wing. Aerodynamic drag was defined for a baseline engine airflow condition, and all propulsion-related effects due to variations from this baseline were accounted for in the corrected flight test data as discussed later in this paper.

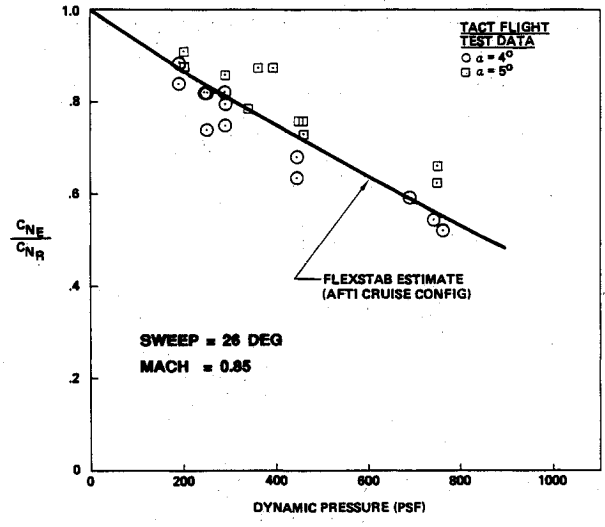

Fig. 4 FLEXSTAB to TACT flight test correlation – normal force.

Drag Component Buildup

Full-scale airplane drag was separated into various components and written in coefficient form as

$$C_{D_{\text{airplane}}} = C_{D_{\text{min}}} + C_{D_{\text{lift}}} + C_{D_{\text{trim}}} + C_{D_{\text{body attitude}}} \tag{3}$$

where

$$C_{D_{\text{min}}} = (C_{D_{\text{min}}})_{\text{wt model}} + \Delta C_{D_{\text{scale}}} + \Delta C_{D_{\text{aero/prop}}} \tag{4}$$

$$C_{D_{\text{lift}}} = (C_{D_{\text{lift}}})_{\text{wt model}} + \text{f(flexibility)} \tag{5}$$

$$C_{D_{\text{trim}}} = (C_{D_{\text{trim}}})_{\text{wt model}} + \text{f(flexibility)} \tag{6}$$

$$C_{D_{\text{body attitude}}} = \text{f(flexibility)} \tag{7}$$

The effect of airplane flexibility on drag was reflected in the drag due to lift [Eq. (5)] and trim drag [Eq. (6)] terms plus a correction for body attitude relative to the wing [Eq. (7)]. Additional details regarding the development of the preceding expressions may be found in Ref. 4.

Trim Drag

In order to minimize wind-tunnel test time, a simple trim routine was devised that minimized the amount of horizontal tail deflection test data required. The procedure consisted of obtaining horizontal tail deflection data for a selected few leading- and trailing-edge flap deflection combinations. Horizontal tail effectiveness, tail moment arm, downwash angles, and tail drag polars were then extracted from tail-on and tail-off wind-tunnel data and flap effects averaged out as shown by the examples in Figs. 7 and 8. Next, flexibility corrections were applied and trimmed drag polars assembled by adding tail trim drag increments to the tail-off lift and drag according to the equations given in Fig. 6. Trimmed drag polars calculated in this manner correlated well with tail-on trim points obtained in the tunnel as shown by the example in Fig. 9.

Wind-Tunnel Test Results

At any given lift coefficient there was an optimum camber setting that could produce minimum drag. The locus of combined variable-camber leading- and trailing-edge flap deflections providing minimum drag as a function of lift coefficient was defined as the variable-camber envelope (Fig. 10). Leading- and trailing-edge flap deflections were programmed as a function of lift coefficient and Mach number in the MCC automatic mode (Fig. 11).

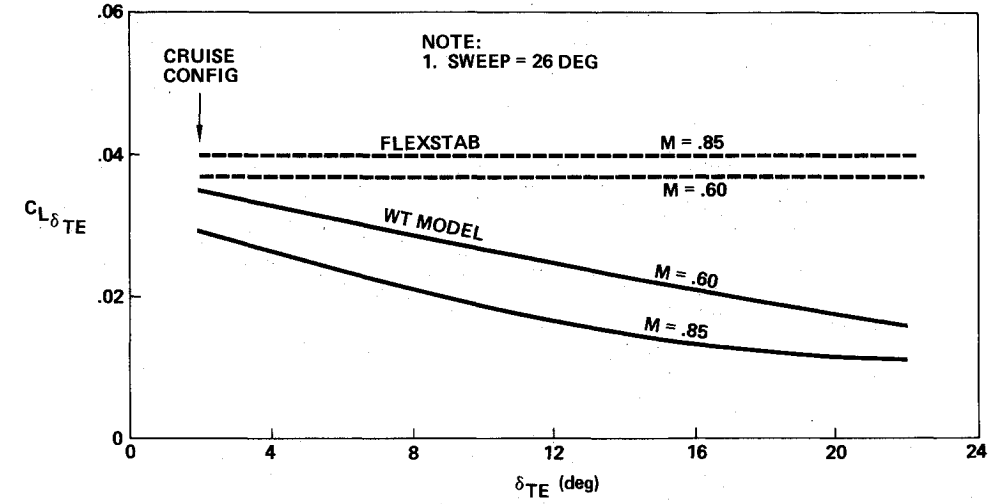

Fig. 5 FLEXSTAB to wind-tunnel correlation – trailing-edge flap effectiveness.

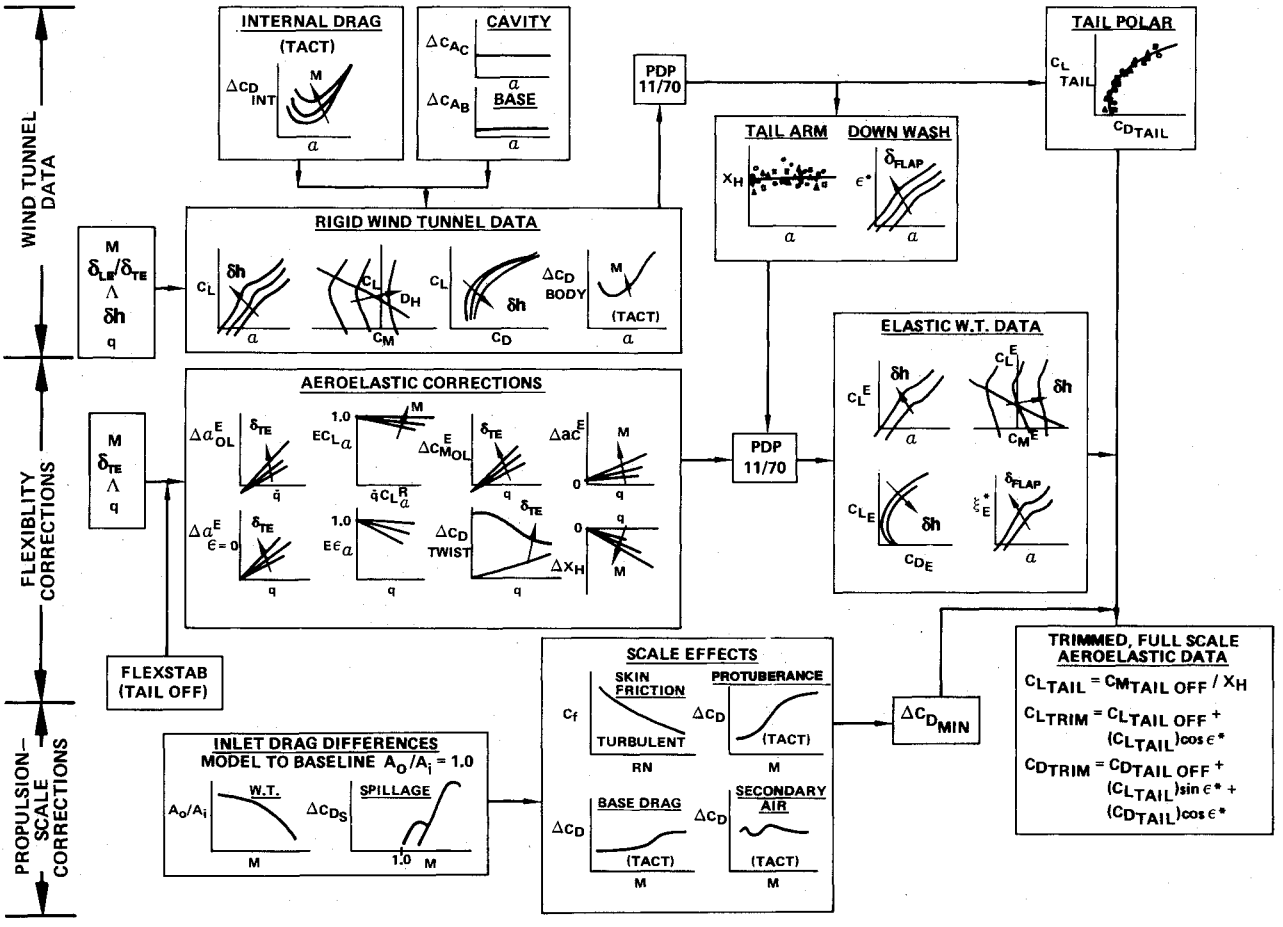

Fig. 6 Full-scale drag buildup.

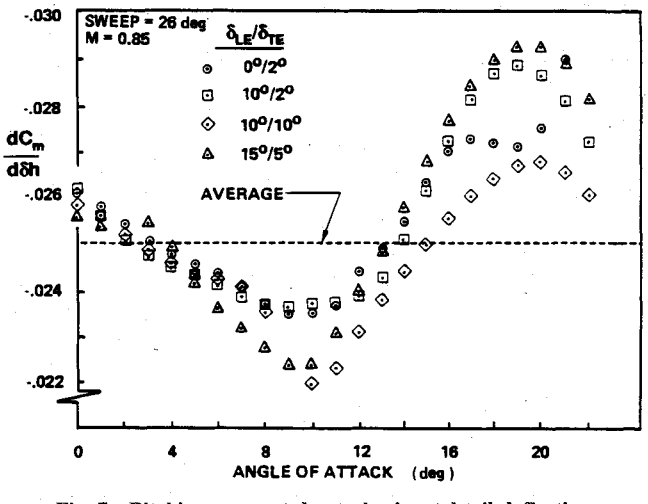

Fig. 7 Pitching moment due to horizontal tail deflection.

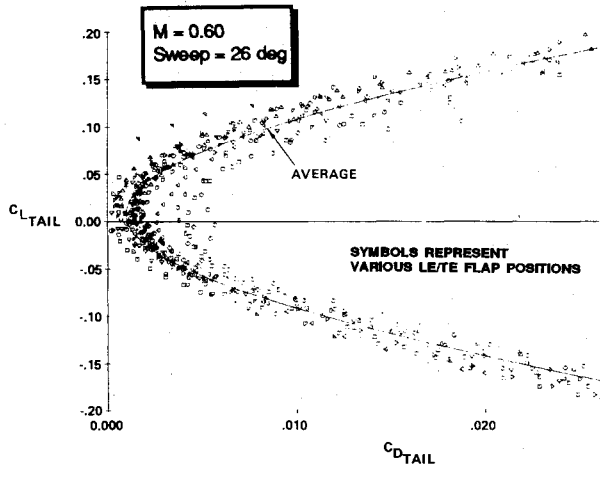

Fig. 8 Tail polar data.

Full-scale variable-camber envelope drag characteristics, derived from wind-tunnel data, are compared against the AFTI cruise wing (W2.4E) and the TACT wing (W54) in Fig. 12. The variable-camber envelope drag benefits (over TACT) were substantial at conditions away from the TACT and AFTI cruise wing design points (0.85 Mach number, $0.45C_L$), especially in the high-lift coefficient region at 0.70 Mach number. This was the result of the variable-camber leading edge reducing a severe leading-edge suction peak and eliminating the associated boundary-layer separation bubble that existed on the AFTI cruise and TACT wings at these conditions. As Mach number was increased, compressibility effects reduced the leading-edge suction peak, thereby limiting the variable-camber advantage. Above 0.85 Mach number, variable-camber drag benefits were further diminished by the formation of local shock waves. The wind-tunnel results were substantiated by flight test as described later.

Flight Test

Test Approach

The choice of test conditions was based on similarity to wind-tunnel test conditions. This approach provided a direct basis for comparison. Testing was concentrated at the cruise wing sweep of 26 deg with lesser amounts of data at the aft

wing sweep of 58 deg. Testing at 26 deg was also concentrated at one dynamic pressure level (300 psf). However, some higher dynamic pressures were looked at to investigate flexibility effects. The LE and TE camber settings chosen were in the range of values most efficient for operation at the flight conditions tested. The aggregate of flight conditions and wing configurations is depicted in Table 1.

The flight test maneuvers were designed to provide data to generate a drag polar for each flight condition and wing configuration. A level flight cruise point was flown, followed by a roller-coaster maneuver at constant Mach number. The latter consisted of a gradual push-over to about 0.5 g, followed by a pull-up to approximately 2.5 g, all flown at the trim throttle setting. The maneuver lasted between 10–20 s and was of short enough duration that Mach number did not bleed off apprecia-

Table 1 Flight test configurations

Wing sweep, deg	Mach no. range	Dynamic pressure, psf	Camber settings, LE deg/TE deg
26	0.70–0.85	300	0/2, 5/2, 5/6, 5/10
26	0.70, 0.85	600, 900	0/2, 5/6, 5/10
26	0.65, 0.87–0.95	300	0/2
58	0.80/0.90	300/600	0/2, 5/6, 10/6
58	1.10–1.30	450	0/2, 0/−1, 10/−1 10/2, 10/6

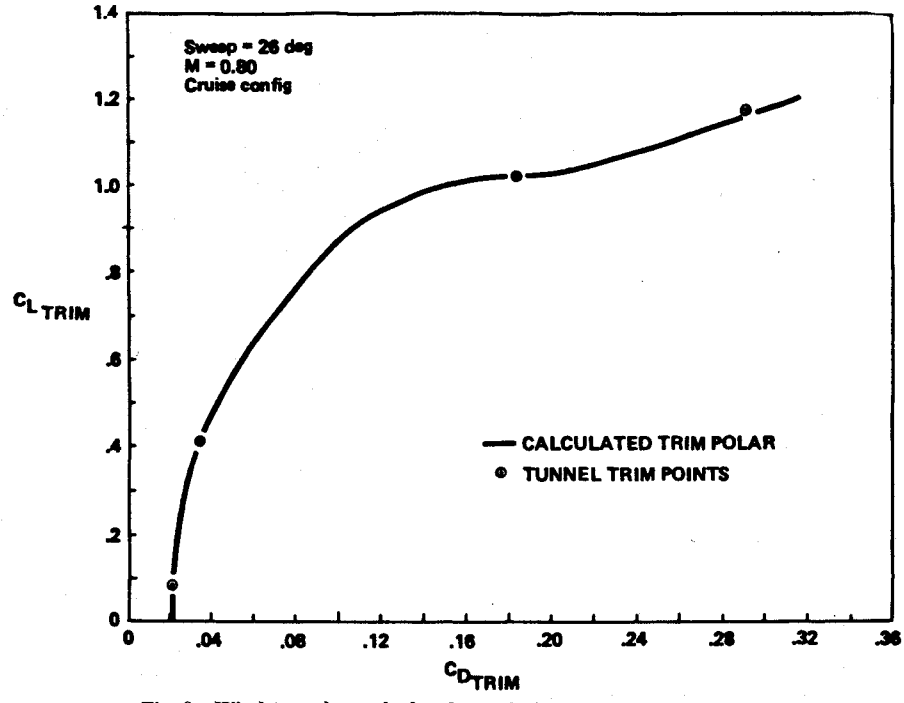

Fig. 9 Wind tunnel to calculated correlation – trimmed drag polar.

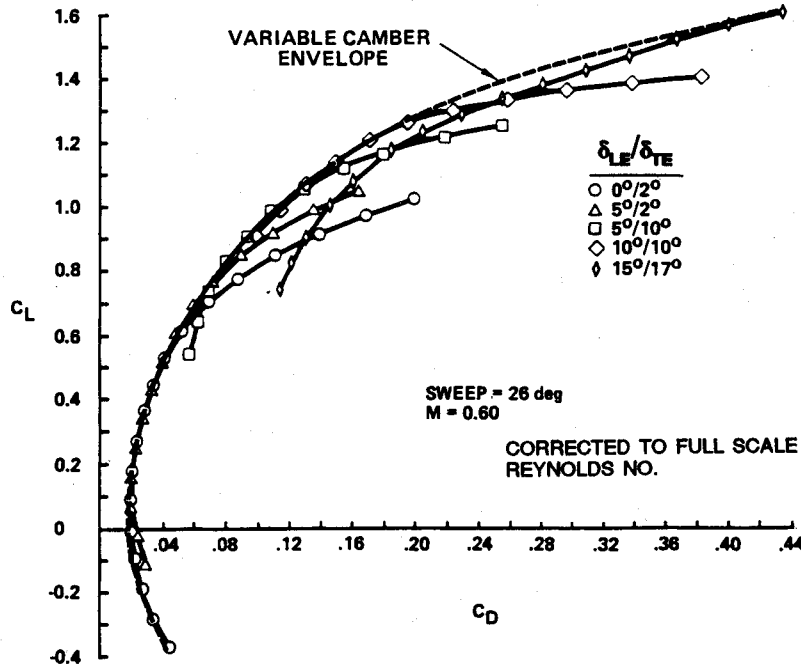

Fig. 10 Wind-tunnel full-scale variable-camber envelope, rigid airplane.

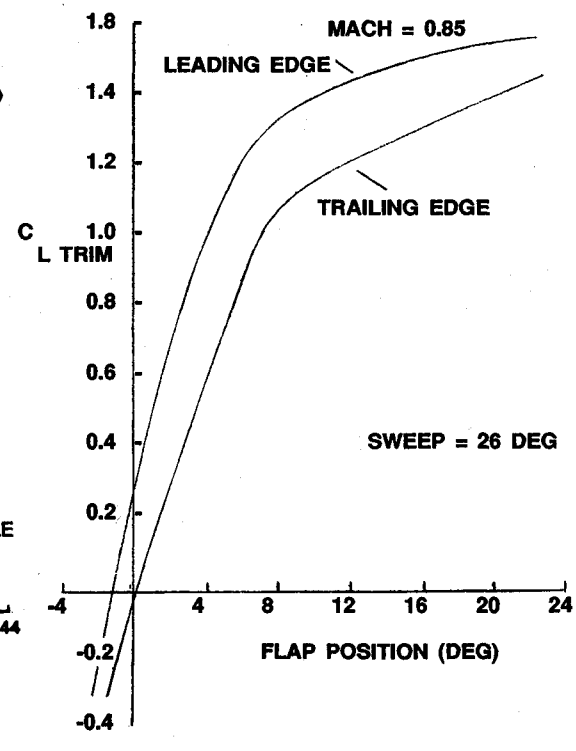

Fig. 11 Maneuver camber flap schedule.

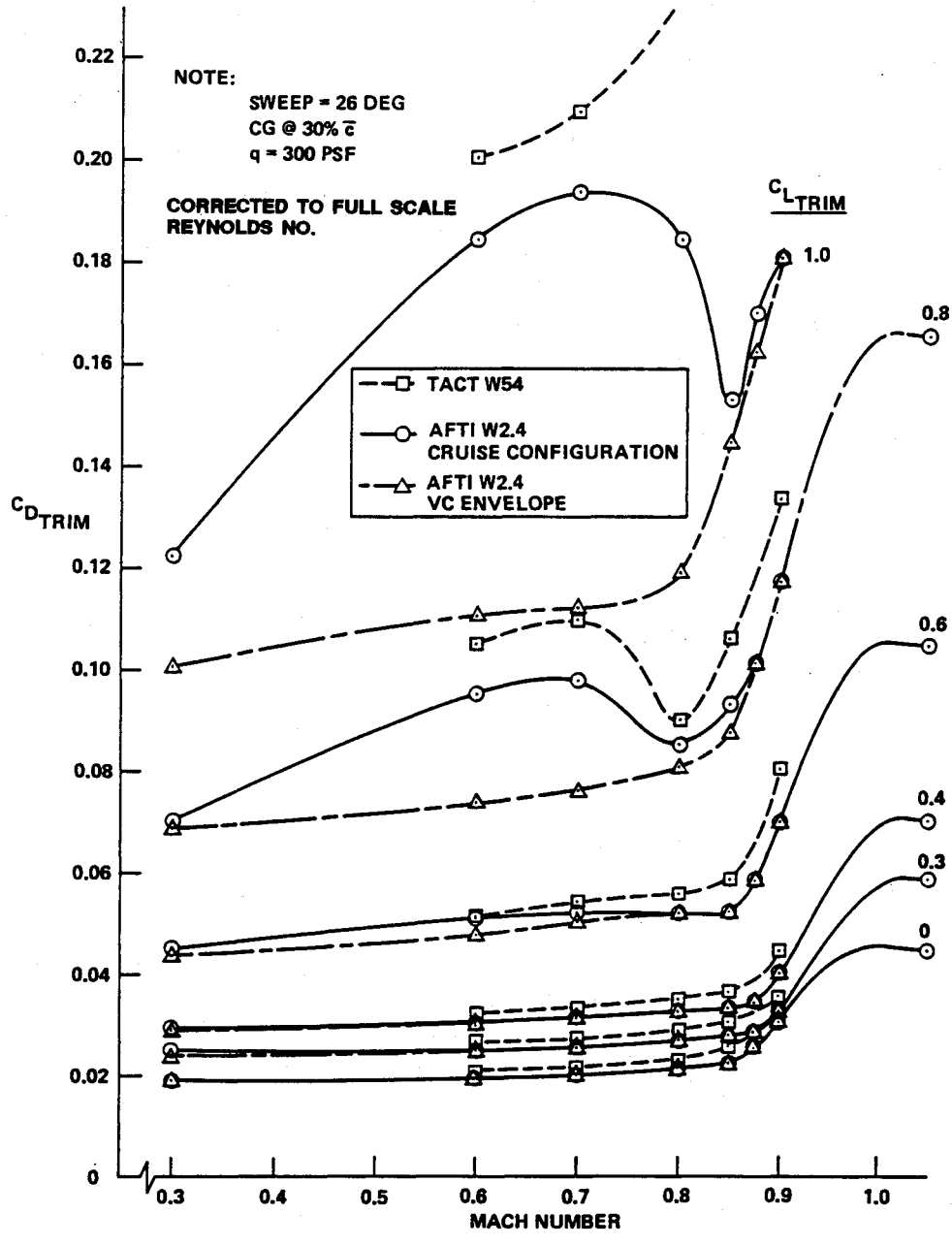

Fig. 12 Effect of variable-camber envelope on trimmed drag from wind tunnel.

bly (≤ 0.01). These maneuvers provided data over a range of lift coefficients from about 0.20 to 1.1. In addition to these two core maneuvers, constant load-factor turns were flown to check against any contamination of the drag results by the dynamics of the roller coasters. In addition to the test maneuvers, calibration maneuvers were flown to assess the noseboom static source position error and the angle-of-attack upwash.

Data Analysis

The calculation of engine thrust and aircraft lift and drag made use of proven techniques. Particular pains were taken to develop and validate accurate flight measurements, thrust calculation procedures, and thrust/drag bookkeeping adjustments. These techniques proved valid and provided in-flight drag results that correlated well with wind-tunnel estimates.

The basic equations used to compute lift and drag were as follows:

$$C_L = [Wn_z - F_g \sin(\alpha_w - i_t)]/qS \quad (8)$$

$$C_D = [F_g \cos(\alpha_w - i_t) - F_e - n_x W]/qS \quad (9)$$

The normal and longitudinal flight-path accelerations (n_z and n_x) were measured using a sensitive, two-axis accelerometer mounted on the angle-of-attack vane shaft on the noseboom. With this arrangement, the accelerometer was kept approximately aligned with the flight path.

To compute thrust of the F-111's TF30-P-9 engines, both engines were instrumented to record primary engine variables such as compressor/fan speeds, nozzle exit temperature/pressure, and nozzle area. The left engine was extensively instrumented to compute bleed and secondary airflows. Gross thrust was computed using a pressure-area method, defined by Pratt and Whitney Aircraft[5] and refined for the TACT program.[6] The required engine mass-flow rates and nozzle discharge conditions were computed from experimentally derived data.[5] An experimentally derived gross thrust coefficient was determined from data provided in Ref. 6 and adjusted using static thrust run measurements conducted on the as-installed engines at the Edwards AFB thrust stand. Adjustments to gross thrust were made to account for secondary cooling airflow and nozzle ejector geometry effects.

Adjustments were required to bring the computed lift and drag to certain reference conditions to allow direct comparison with wind-tunnel estimates. These adjustments included afterbody force corrections (throttle effects), spillage drag increments, and trim drag increments:

Afterbody effects. These pressure forces resulting from the engine exhaust stream were computed from TACT wind-tunnel results. The correction term referenced this force component to a cruise flight condition at 30,000 ft. Computed gross thrust was adjusted by this additive correction.

Spillage drag. The spillage drag increment between an actual, computed capture area ratio and a reference capture area ratio of 1 was computed and added to the calculation of drag.

Trim drag. Corrections were made from the as-flown, untrimmed maneuver to a trimmed, stable flight condition and also to a chosen reference center of gravity (c.g.) position. The reference c.g. positions corresponded to a midgross weight and were peculiar to each test wing sweep position. These adjustments entailed computing an increment in horizontal tail position and the resulting change in trim lift and drag. Boeing wind-tunnel data were used to determine these corrections.

Data repeatability was checked during the flight program as a way of building confidence in the quality of the results. Repeat maneuvers were flown as time permitted on different flights, and the maximum amount of scatter observed was approximately ± 15 drag counts (in this case for four repeated roller coasters). This was considered acceptable for the purposes of the program. In addition, drag data computed for stabilized level flight points, roller coasters, and stabilized turns were compared. The data from these three sources all fell well within the polar scatter band with very little deviation. An example of drag polar data is presented in Fig. 13. Maneuver dynamics and throttle differences, thus, had little influence on the results.

Flight Test Results

Flight and wind-tunnel comparisons are shown in Figs. 14 and 15. In general, the flight-derived aircraft drag agreed fairly well with wind-tunnel estimates—within about 20 drag counts for a wing sweep of 26 deg. They were neither consistently higher nor lower than wind-tunnel results. There were some notable exceptions, however. For example, at a Mach number

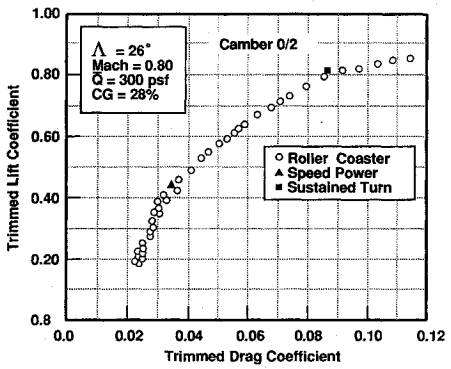

Fig. 13 Drag polar flight data.

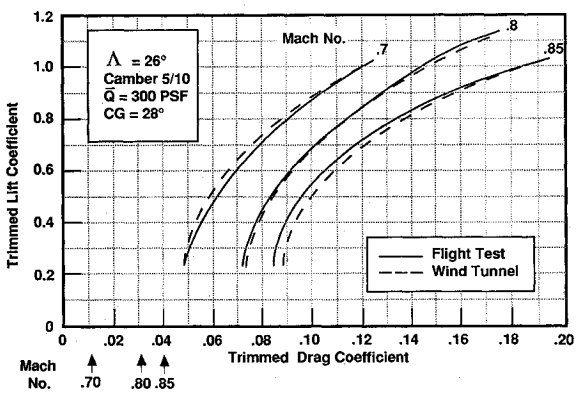

Fig. 14 Drag polar comparison, 26-deg sweep.

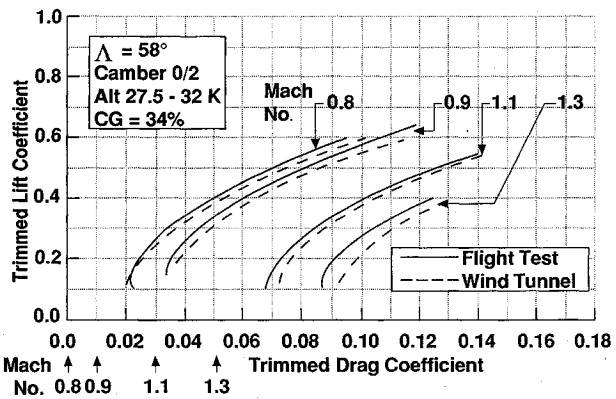

Fig. 15 Drag polar comparison, 58-deg sweep.

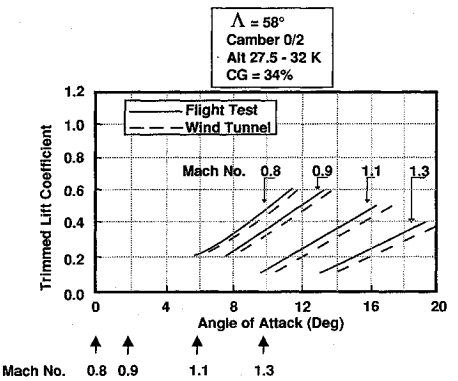

Fig. 16 Flight test to wind-tunnel comparison – trimmed lift.

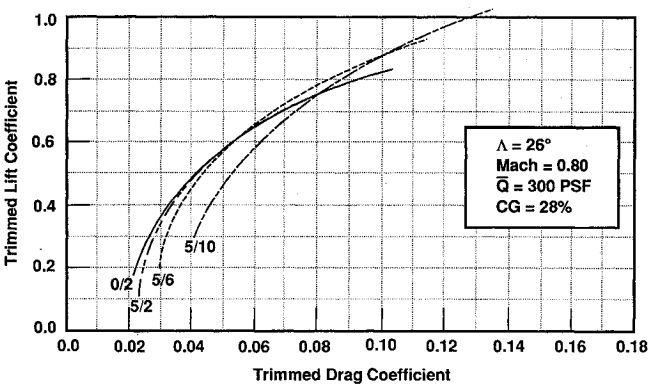

Fig. 17 Flight test variable-camber envelope generation.

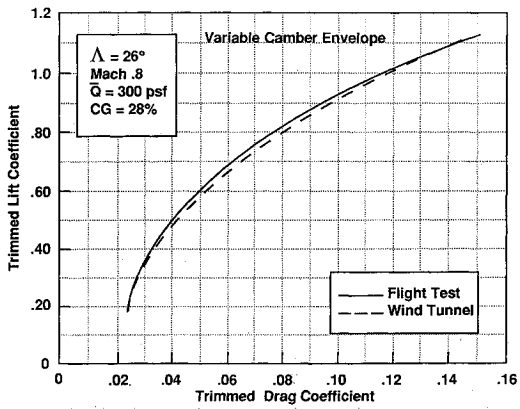

Fig. 18 Flight test to wind-tunnel comparison – variable-camber envelope, 26-deg sweep.

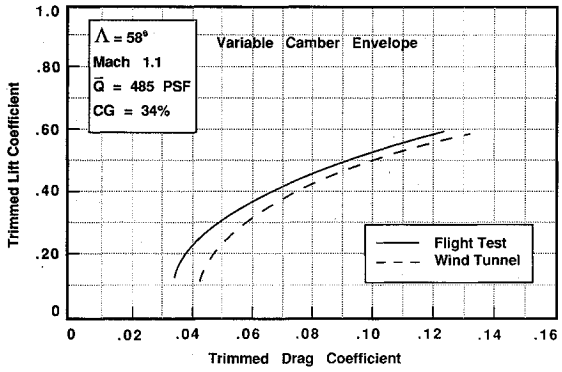

Fig. 19 Flight test to wind-tunnel comparison – variable-camber envelope, 58-deg sweep.

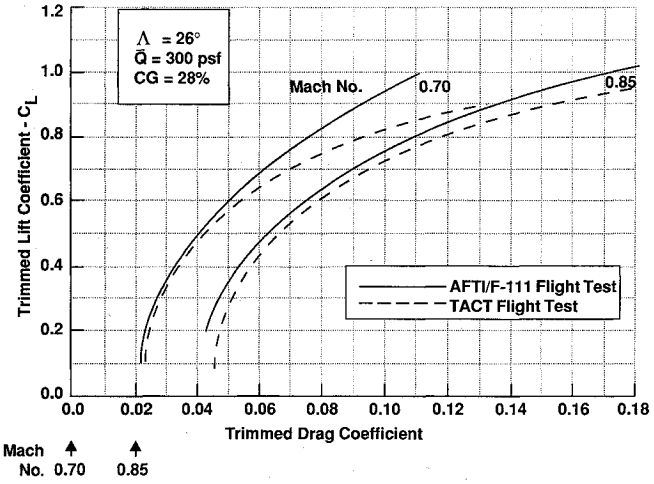

Fig. 20 AFTI to TACT flight test comparison – drag polar.

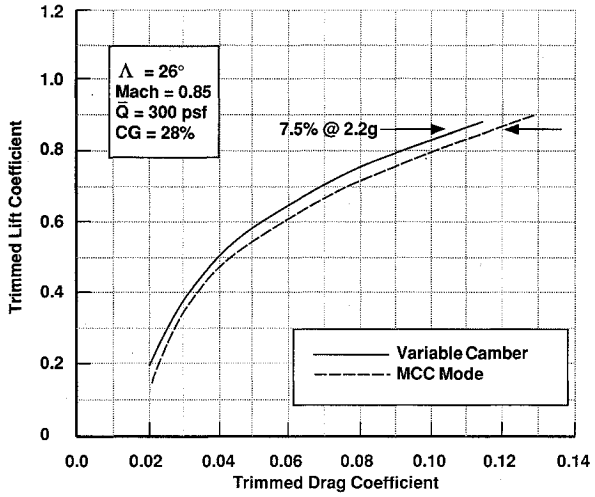

Fig. 21 MCC mode drag polar.

of 0.85 and a wing sweep of 26 deg, flight test drag levels were lower than estimated by up to 60 counts. Lower flight drag was also evident at 58-deg sweep for all of the Mach numbers tested. For these cases, the drag polar shapes generally compared, with no consistent differences noted, indicating there was a shift in C_{D0}. A clue to this behavior was seen in the wind-tunnel/flight test comparisons of trim horizontal tail position and trim lift. Flight test showed both a lower trim angle of attack (0.50–1.0 deg) and a smaller amount of trim tail required (2–3 deg). The lift curve slope agreed reasonably well indicating that the zero-lift angle of attack was in disagreement. One angle-of-attack comparison is shown in Fig. 16.

In addition to discrete camber polars, the optimum variable-camber envelope was generated for several flight conditions at both wing sweeps, as was done for wind-tunnel data. An example is shown in Fig. 17, similar to the wind-tunnel composite fairings of Fig. 10. As seen in Fig. 18, there was a quite close match between the 26-deg wind-tunnel and flight tests. For 58 deg (Fig. 19), the lower drag of the flight test data was evident.

Comparison with TACT

Comparisons were also made with the basic TACT wing to illustrate the potential improvements provided by the MAW, using the variable-camber envelope as a basis for comparison. The wing reference area for both AFTI and TACT was the same: 603.9 ft^2. Figure 20 shows the significant reduction in drag afforded by the MAW. The refined supercritical airfoil design was responsible for the drag reduction in the cruise regime ($C_L = 0.4$, Mach = 0.85), whereas the smooth, variable camber reduced drag at off-design conditions, as explained earlier. The drag reduction varied from 7.6% at the design cruise point to over 20% at an off-design condition ($C_L = 0.8$, Mach = 0.75).

Maneuver Camber Control

Results were also obtained with the MCC automatic mode engaged. Windup turn and roller-coaster maneuvers were flown to obtain drag polars in the MCC to compare with the derived, variable-camber envelope polar, which the mode was intended to match. Good agreement would indicate that the table lookup cambers were close to the optimum and that dynamic effects, due to continuous movement of the flaps in the maneuver, were negligible. Figure 21 illustrates one comparison. The MCC mode showed somewhat higher drag at the higher lift coefficients. This was attributed to the stored table camber values being slightly in error. Dynamic effects due to aerodynamic or camber scheduling lag were found to be negligible.

Concluding Remarks

The expected drag improvements due to smooth, variable-camber geometry were demonstrated by both wind-tunnel and flight tests. The largest improvements in drag occurred at off-design conditions where the MAW's ability to smoothly reconfigure itself showed its maximum advantage. The utility of a control mode to automatically position this type of wing to its optimum, minimum drag camber was demonstrated. The generally good agreement between wind-tunnel and flight tests, particularly for 26-deg wing sweep, allowed a minimum flight test data base in order to adequately map the performance characteristics over the flight envelope. This approach reduced the required amount of flight testing to fit within program constraints.

References

[1]Bonnema, K., and Smith, S., "AFTI/F-111 Mission Adaptive Wing Flight Research Program," AIAA Paper 88-2118, May 1988.

[2]Tinoco, E. M., "FLEXSTAB – A Summary of the Functions and Capabilities of the NASA Flexible Airplane Analysis Computer System," NASA CR-2564, Dec. 1975.

[3]Woodward, F. A., "Analysis and Design of Wing-Body Combinations at Subsonic and Supersonic Speeds," *Journal of Aircraft*, Vol. 5, No. 6, 1968, pp. 528–534.

[4]Smith, S., and Nelson, D., "Determination of the Aerodynamic Characteristics of the Mission Adaptive Wing," AIAA Paper 88-2556, June 1988.

[5]"In-Flight Performance Determination for TF30-P-7 and TF-30-P-9 Engines," Pratt and Whitney Aircraft Division of United Aircraft Corp., East Hartford, CT, PWA-3994, Oct. 1970.

[6]Cooper, J., Hughes, D., and Rawlings, K., "Transonic Aircraft Technology Flight-Derived Lift and Drag Characteristics," Vol. I, Air Force Flight Test Center, Edwards AFB, CA, AFFTC-TR-77-12, July 1977.